The Spectral Shape and Photon Fraction as Signatures of the GZK Cut-Off

Andrew M. Taylor

Max-Planck-Institut für Kernphysik, Postfach 103980, D-69029 Heidelberg, GERMANY

Felix A. Aharonian

Max-Planck-Institut für Kernphysik, Postfach 103980, D-69029 Heidelberg, GERMANY and
Dublin Institute for Advanced Studies, 5 Merrion Square, Dublin 2, IRELAND

With the prospect of measuring the fraction of arriving secondary photons, produced through photo-pion energy loss interactions of ultra high energy cosmic ray (UHECR) protons with the microwave background during propagation, we investigate how information about the local UHECR source distribution can be inferred from the primary (proton) to secondary (photon) ratio. As an aid to achieve this, we develop an analytic description for both particle populations as a function of propagation time. Through a consideration of the shape of the GZK cut-off and the corresponding photon fraction curve, we investigate the different results expected for both different maximum proton energies injected by the sources, as well as a change in the local source distribution following a perturbative deformation away from a homogeneous description. At the end of the paper, consideration is made as to how these results are modified through extra-galactic magnetic field effects on the proton's propagation. The paper aims to demonstrate how the shape of the cosmic ray flux in the cut-off region, along with the photon fraction, are useful indicators of the cut-off origin as well as the local UHECR source distribution.

I. INTRODUCTION

Ultra high energy cosmic rays with energies $\sim 10^{19}$ eV arrive at Earth with a frequency of less than ~ 1 km^{-2} yr^{-1} (ie. with an energy flux of 30 eV cm^{-2} s^{-1}) in π sr. The now complete Pierre Auger detector (Auger) [1], covering ~ 3000 km^2 in area, is able to detect several hundred cosmic ray events per year at energies $\sim 10^{19}$ eV. At energies around 10^{20} eV, the arrival frequency reduces to below 0.01 km^{-2} yr^{-1}, with only a few events per year expected to be detectable by Auger. This demonstrates both the low luminosity of the arriving UHECR "beam" and the relatively good statistics achievable by Auger. Thus, the arrival of these extremely large detectors allows more to be inferred than simply the presence of the cut-off in the arriving UHECR spectrum.

Before their arrival, these UHECR must propagate across the astronomical distances between their source and Earth. Though their composition remains unclear [2], it seems reasonable to assume that they contain a proton component. In this paper we will ignore a nuclei component in our discussion of UHECR. A description of the propagation of heavier nuclear species up to iron can be found in ref. [3, 4, 5]. With the $p\gamma$ pair production and pion production cross-sections both rising quickly above the threshold values of 1 MeV and 145 MeV respectively (these photon energies being in the proton's rest-frame), once sufficient center-of-mass energy is available in the collisions, these processes become of relevance to UHECR protons during their propagation to Earth, and they begin to lose energy through these particle production channels.

At the high energy end of the UHECR spectrum, the required center-of-mass energy for both pair ($p\gamma \rightarrow pe^+e^-$ [6]) and pion production ($p\gamma \rightarrow p\pi^0/n\pi^+$ [7, 8]) is found through collisions of the UHECR with both 2.7 K cosmic microwave background (CMB), whose energy density peaks with photons of energy $\sim 10^{-3}$ eV, and to a lesser extent with the infra-red background, whose energy density peaks with photons of energy $\sim 10^{-2}$ eV. Provided the propagation time from their sources to Earth is greater than their energy loss time, the protons invariably undergo these energy loss interactions, generating a secondary flux of ultra high energy (UHE) electrons, photons, and neutrinos en-route, sharing out their energy flux among these various "stable" particle types via these particle production processes. In the left-panel of fig. 1, we show the calculated energy loss lengths for UHECR in the energy range under consideration, the determination of which is explained in ref. [3].

Isotropy is observed in the arriving UHECR distribution detected by Auger for energies below $\sim 10^{19.7}$ eV, though above this energy there appears to be evidence (at the $\sim 3\sigma$ level) for a departure from isotropy [9]. Such a departure signal is naturally expected to occur in this energy range following the reduction of the UHECR energy loss lengths at these energies, approximately describable by [10, 11]

$$l_{\text{horiz.}} = \frac{l_0 e^x}{(1 - e^{-x})} \tag{1}$$

where $l_0 = 5$ Mpc, $x = E_{p,0}/E_p$ and $E_{p,0} = 10^{20.53}$ eV. This description gives a good approximation to the proton photo-pion loss lengths, for interactions with the CMB only, in the range $1 < x < 10$. With the UHECR above
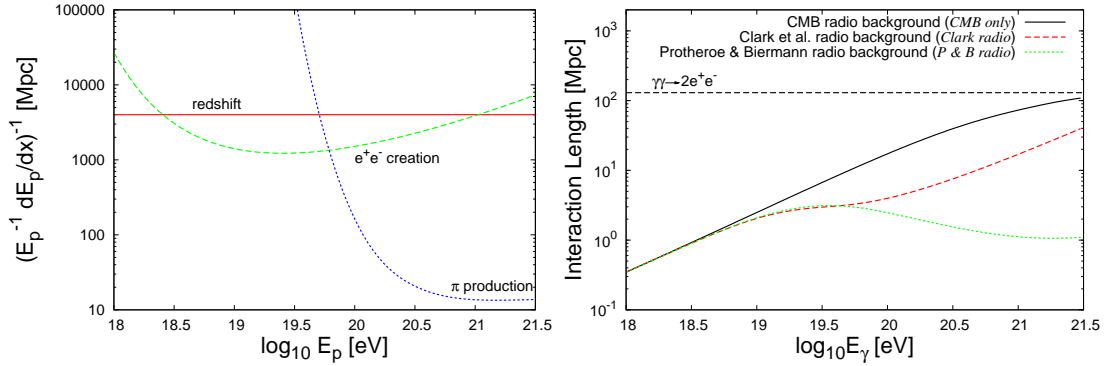
FIG. 1: **Left**: The energy loss lengths lengths through redshift, pair creation, and pion production, for UHECR protons propagating through the cosmic microwave background radiation field. **Right**: The interaction lengths for UHE photons propagating through the cosmic microwave and radio background radiation fields.

$10^{19.6}$ eV arriving from increasingly more local sources, the overall deflection angle of the arriving UHECR, from that at which they were emitted, is thus expected to reduce. Furthermore, for a given magnetic field strength, the UHECR Larmor radius increases with proton energy, resulting in less deflection during propagation from a given source for higher energy particles.

Along with a correlation of the UHECR arrival directions with the local distribution of AGN, the shape of the GZK [7, 8] feature itself contains information about the source distribution [12, 13]. As the cosmic rays produced by these sources are attenuated via pion-production interactions with the background radiation field photons, a subsequent flux of UHE photons, following the decay of the neutral pions, is produced. However, unlike the flux of high energy (cosmogenic) neutrinos produced through the decay of the corresponding charged pion component, previously discussed in ref [14, 15, 16], UHE photons produced via the neutral pion decay are not free to propagate through the Universe over cosmological distances unimpeded since they also interact with the background photon field via $\gamma\gamma \rightarrow e^+e^-$ [17] on $\sim$Mpc size scales (see right-hand panel of fig.1), thus their flux is attenuated on scales similar to that on which they are produced through high center-of-mass $\gamma\gamma$ collisions. These UHE electrons, produced through $\gamma\gamma$ pair production, may then go on to either inverse Compton cool [18] off the background photon fields through high center-of-mass $e\gamma$ collisions, leading to a repeating cycle of pair production and inverse Compton scattering and the development of an electromagnetic (e/γ) cascade [19, 20, 21], or to synchrotron cool in the extra-galactic magnetic field. The dominance of one of these processes depending on both the level of the cosmic radio background and the magnitude of the extra-galactic magnetic field [22, 23].

With no prior knowledge about the UHECR source population, a vanilla sky homogeneous and isotropic distribution is naturally assumed. We use such an assumption as our starting point in this paper, departing from this assumption in a perturbative way so as to explore the effects introduced by such departures into the arriving proton and photon fluxes. With $> 10^{18}$ eV protons energy loss scales being 10-1000 Mpc and $> 10^{18}$ eV photons energy loss scales being 1-100 Mpc, and source distance scales expected $\sim$50 Mpc, the UHECR proton and photon fluxes collectively are perfectly suited to use as a probe of the local source distribution.

In order to quantify the effects of different source distributions in this paper, we separate out the fluxes produced from source regions with shells of radii 0-3 Mpc, 3-9 Mpc, 9-27 Mpc, 27-81 Mpc, and 81-243 Mpc surrounding the Earth. In this way, the results obtained may be used to encapsulate the effects introduced by a local over-density or under-density of UHECR sources. As the ultimate fate of the energy flux injected into the UHE photon population by our UHECR population is dependent upon both the strength of the background radiation field at radio energies, 10^{-8}-10^{-6} eV, and the extra-galactic magnetic field strength, we account for the different eventualities the energy propagation through the system may follow through a consideration of extreme cases.

Previous investigations into the photon flux produced through GZK interactions [19, 22, 23], have demonstrated that significant photon fractions can be expected for particular assumptions about the UHECR sources and extra-galactic environment. We demonstrate here that the photon fraction naturally provides a complimentary measurement to that of the spectral cut-off feature, allowing differentiation between the "tired source" and GZK cut-off scenarios as well as carrying information about the distribution of the local UHECR source population. We aid our discussion with the development of an analytic description of the proton and photon fluxes, which provides a clear understanding of our results. With Auger measurements of the arriving UHECR flux already probing the photon fraction down to values $\sim 10^{-2}$, and the possibility to probe even smaller fractions [24], the crucial complimentary information this will
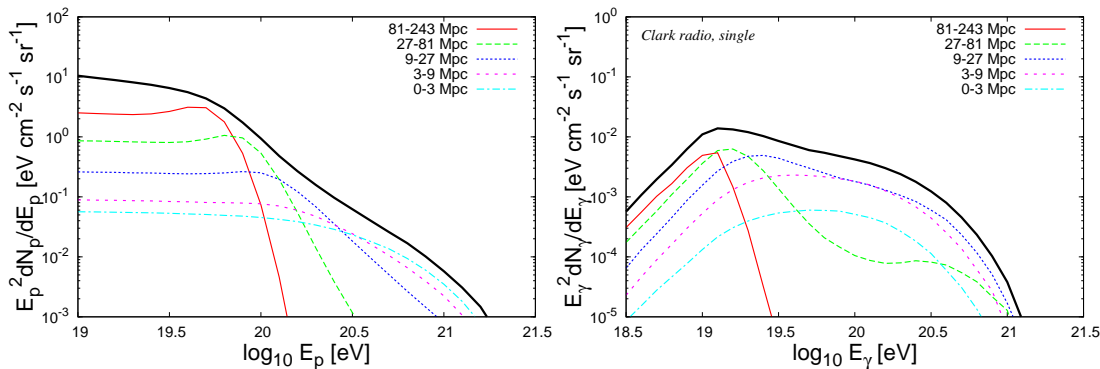
FIG. 2: **Left**: A breakdown of the arriving UHECR proton flux from different injection shell radii. **Right**: A breakdown of the arriving UHE photon flux from different injection shell radii. For this flux, the label "*Clark radio, single*" refers to the assumptions about the radio background and magnetic field strengths, for which we have assumed the Clark et al. [25] radio background and extra-galactic magnetic fields stronger than 0.1 nG. The injected proton spectrum assumed for these results had a cut-off energy of $E_{max}=10^{20.5}$ eV and an injection spectral index of $\alpha=2$.

provide to the spectral UHECR measurements holds great promise.

In section II we consider the contribution to both the arriving UHECR flux and arriving UHE photon flux from different source shells. An analytic description for both these fluxes is derived. We go on to highlight the dependence of the photon flux on the cosmic radio background and extra-galactic magnetic field strengths assumed. In section III we obtain the photon fraction for the case of a homogeneous distribution of sources. We then demonstrate the role that the cut-off energy, E_{max}, plays in this photon fraction result. Following this we investigate the effect different local source distributions would have on the spectral-shape of the cut-off and the photon fraction of the arriving UHECR flux. The section ends with the consideration of the extreme case of the development with distance of the photon fraction from a single source. In section IV we discuss how diffusion of the UHECR would affect the results obtained. We discuss a summary of our results in section V, making our conclusions in section VI.

II.   PROTON AND PHOTON FLUXES FROM A UNIFORM DISTRIBUTION OF SOURCES

In this section we assume that the UHECR sources have a homogeneous density distribution locally, with the number of sources scaling simply with the co-moving volume element under consideration. Along with this, we assume each source is producing UHECR with a power law energy spectrum and an exponential cut-off. These source spatial and energy distributions are given by

$$\frac{dN}{dV_c} \propto (1+z)^3 \qquad\qquad \frac{dN}{dE} \propto E^{-\alpha}e^{-E/E_{max}} \qquad (2)$$

respectively, with $\alpha=2$ and $E_{max} = 10^{20.5}$ eV, unless otherwise stated. Following these assumptions, the arriving proton and photon fluxes are shown in fig. 2.

The proton fluxes from the different source shells, shown in the left-panel of fig. 2, demonstrate simply how each shell has an energy range at which it contributes the dominant flux component of the arriving UHECR. Accompanying the arriving proton flux, we also show the arriving photon flux in the right-panel of fig. 2, produced en-route after the protons have left the source region, typically after a distance $l_{horiz.}$ (see eqn (1)). For the photon flux arriving from the more distant shells (>27 Mpc), a clear dip feature can be seen to exist at energies of $\sim 10^{20}$ eV. This feature originates from the sudden increase in the pion production rate $\sim 10^{19.6}$ eV, as seen in dotted energy-loss length curve in the left-panel of fig. 1, occurring when the protons have sufficient Lorentz factors that the populous CMB photons have sufficient energy to excite their delta resonances. Since, when this occurs, the average distance at which the pions are produced from the emitting shell drops as $e^{E_{p,0}/E_p}$, the source region disappears behind the pair production horizon leading to the sudden falling part seen before the dip feature. At higher energies the pair production horizon increases leading to the slower rising part after the dip feature.
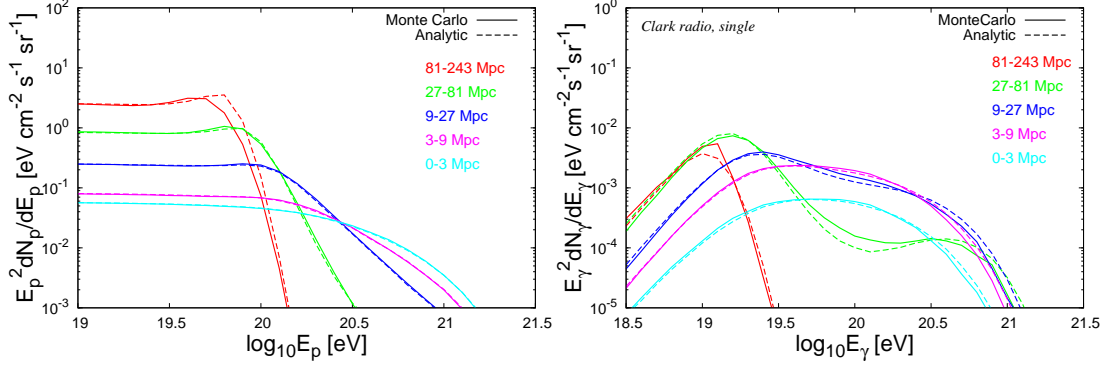
FIG. 3: **Left**: A comparison of the analytic description for the GZK feature of the proton flux with the complete Monte Carlo description. **Right**: A comparison of the analytic description given above for the photon flux produced during UHECR proton propagation with the complete Monte Carlo description. For this flux, the label "*Clark radio, single*" refers to the assumptions about the radio background and magnetic field strengths, for which we have assumed the Clark et al. [25] radio background and extra-galactic magnetic fields stronger than 0.1 nG. To obtain both sets of analytic results the formalism in section II A was used. The injected proton spectrum assumed for these results had a cut-off energy of $E_{\max}=10^{20.5}$ eV and an injection spectral index of $\alpha=2$.

A. Analytic Description for the UHE Proton and Photon Fluxes

The shape of the GZK feature, the shell contributions to which are shown in the left-hand panel of fig. 2, carries valuable information about the local source distribution. A simple analytic description of this feature, found in ref. [26, 27], allows the different cut-offs in the fluxes from the various shells to be interpreted easily. The derivation of this analytic result is explained in ref. [4]

The contribution function, for protons contributing to the arriving flux with energy E_p, written as a function of the total propagation distance L from the source, for proton's having already undergone n pion production interactions, but which have yet to undergo their $(n+1)^{\mathrm{th}}$ pion production process, is given by,

$$\frac{N_n(E_p, L)}{N_0(E, 0)} = \sum_{m=0}^{n} l_0 l_m^{n-1} \exp\left(-\frac{L}{l_m}\right) \prod_{p=0(\neq m)}^{n} \frac{1}{l_m - l_p} \tag{3}$$

where $l_m = l(E_p/(1-K_p)^m)$ is the pion production interaction length for a proton of energy $E_p/(1-K_p)^m$. K_p, the pion production inelasticity, may be approximated as $K_p = 1/2(1 - (m_p^2 c^4 - m_\pi^2 c^4)/s)$ [28], for the energy range of interest, where s is the invariant squared center-of-mass energy of the collision, m_p is the proton rest-mass, and m_π is the pion rest-mass. A simple analytic expression describing $l(E_p)$ for proton interactions with the CMB alone is given in eqn (1) with $l_0 = 1$ Mpc, $x = E_{p,0}/E_p$ and $E_{p,0} = 10^{20.53}$ eV, which provides a good description up to proton energies $\sim 10^{20.5}$ eV.

Combining expressions (1) and (3), summing over $n_{\max}$ different pion loss contribution functions for the flux from the source, the total proton flux from a single source, at distance L is,

$$\frac{dN_{\mathrm{total}}(E_p, L)}{dL} = \sum_{n=0}^{n_{\max}} \frac{N_n(E_p, L)}{N_0(E, 0)}. \tag{4}$$

Integrating L over the relevant source distribution distance range, the total proton flux from the UHECR source production region is obtained. This gives a reasonable analytic description of the GZK-feature, as demonstrated in the left-panel of fig. 3. The discrepancy between the analytic and Monte Carlo description, seen in the plot, for protons from the most distant shell (81-243 Mpc) being due to the neglection of pair losses whose role becomes more important when >100 Mpc propagation distances are probed. This can be understood from the "e^+e^- creation" curve in the left-panel of fig. 1 which demonstrates that loss lengths of a few 1000 Mpc, through proton pair losses in the CMB, are expected. Since the injection spectral index, α, of the UHECR produced by the sources only comes into the calculation of the arriving flux through the weighting factor in the sum over the different pion loss contributions (ie. the different m in eqn (3)), the spectral index is found to play a very minor role in the spectral slope of the GZK feature. Hence, the effect of a steeper spectral index on the arriving proton spectra is simply to steepen the
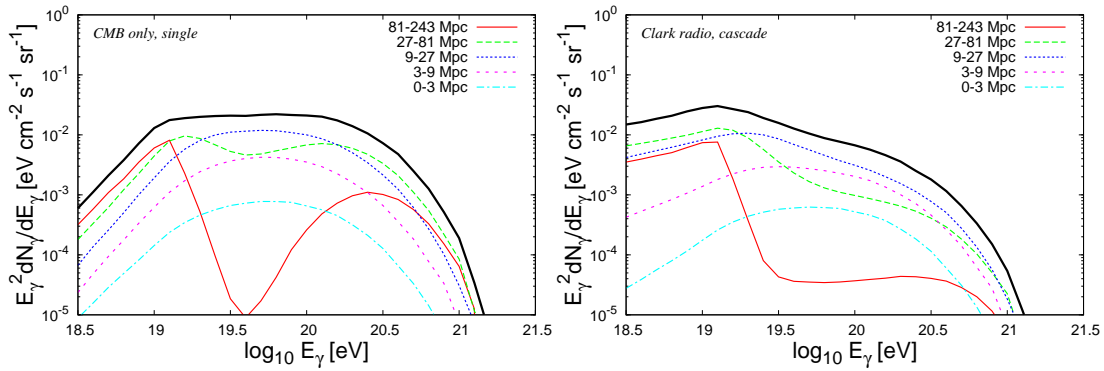
FIG. 4: **Left:** A breakdown of the arriving UHECR photon flux from different injection shell radii for the case of a low radio background and relatively strong magnetic field, "*CMB only, single*". **Right:** A breakdown of the arriving UHECR photon flux from different injection shell radii of for the case of a relatively strong radio background and weak magnetic field, "*Clark radio, cascade*)". The injected proton spectrum assumed for these results had a cut-off energy of $E_{\max}=10^{20.5}$ eV and an injection spectral index of $\alpha=2$.

arriving flux at energies below the GZK feature. Thus, with a smaller energy flux of protons injected into the UHE-photon population in the GZK energy range, a reduced energy flux is injected into the UHE-photon population at the energies around the beginning of the cut-off ($10^{19.6}$ eV), with the injected energy flux reduced further still at even higher photon energies.

A calculation of the arriving photon spectrum produced via neutral photo-pion production interactions of the UHECR protons is a little more involved, requiring the consideration of their production as well as their attenuation through subsequent pair production interactions. In analogy with the production of secondary protons for photo-nuclear disintegration given in ref. [4], the spectrum of neutral pions produced through photo-pion production after having propagated distance L' from the source is given by,

$$N_\pi(L', K_p E_p) = \int_0^{L'} dL \sum_{n=0}^{n_{\max}} \frac{N_n(E_p, L)}{l_n}. \tag{5}$$

Hence, the spatial distribution of neutral pions produced through the propagation of an ensemble of given energy protons, over the entire range in L of source distances under consideration, is obtained. A comparison of the arriving photon flux (following the rapid decay of the neutral pions to photons) from the Monte Carlo and analytic descriptions is shown in the right-hand panel of fig. 3.

B. The Impact of Different Cosmic Radio Background and Extra-galactic Magnetic Field Strengths

In the calculations presented in the right-panel of fig. 2, the propagation of the energy in secondaries soley in the form of photons through the system was implicitly assumed, with the energy of the pair creation electrons disappearing from the system through the synchrotron channel. However, with the present degree of uncertainty in the strengths of the cosmic radio background and extra-galactic magnetic fields, the favoured route that this energy takes also remains uncertain. Following the photon fluxes obtained in the previous section, we here demonstrate the variation introduced by either a weaker radio background or weaker extra-galactic magnetic field strength.

We consider the extreme cases of: a low radio background (dominated by the low energy CMB) and single pair production after which the energy disappears from the system through the synchrotron channel (considering throughout only photon energies above 10^{18} eV); a large radio background [25] and single pair production with electrons cooling via the synchrotron channel; a large radio background and full e/γ cascading. For the second of these, the electron inverse Compton interaction lengths and both electron inverse Compton and photon pair production inelasticities were calculated [29, 30] and a Monte Carlo description of the cascade was used. We refer to this radio background measurement result as large due to possible local foreground contamination from synchrotron emission in the Milky Way's halo. Following radio background measurements, nearly 40 years ago, attempts have been made to model total radio background emitted by sources [31]. However, for the case of a weaker radio background, we consider the extreme case for which the low energy (radio) CMB component is the dominant contribution. Though this scenario is certainly extreme, we use it here simply to demonstrate the effects from a range of parameter space. We refer to
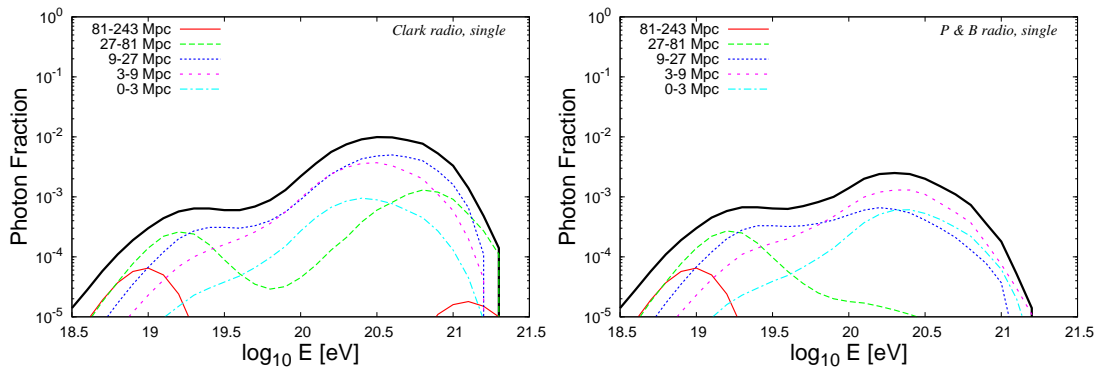
FIG. 5: **Left:** A breakdown of the arriving UHE photon fraction. The label "*Clark radio, single*" refers to the assumptions about the radio background and magnetic field strengths, for which we have assumed the Clark et al. [25] radio background and extra-galactic magnetic fields stronger than 0.1 nG. **Right:** A breakdown of the arriving UHE photon fraction. The label "*Protheroe & Biermann, single*" indicates the the Protheroe & Biermann radio background [31] and extra-galactic magnetic fields stronger than 0.1 nG.For these plots a homogeneous distribution of sources were assumed, each source outputting a proton spectrum with a cut-off energy of $E_{\max}=10^{20.5}$ eV and an injection spectral index of $\alpha=2$.

this scenario as "*CMB only, single*", presenting the results in the left-hand panel of fig. 4. As in the previous section for which the "*Clark radio, single*" scenario was used, a dip feature is seen in the arriving photon flux from the more distance shells (>27 Mpc). The origin of the feature is the same as that described previously (see the beginning of section II). For the case of a weaker extra-galactic magnetic field, we consider the case of sufficiently weak magnetic fields such that the e/γ cascade's development is unhindered. In this scenario, synchrotron cooling times of UHE electrons are slower than the inverse Compton cooling times on the background radiation fields. With synchrotron cooling times going as, $c\tau_{\mathrm{sync.}} = 400 \text{ Mpc} \left(\frac{10^{-11}\mathrm{G}}{B}\right)^2 \left(\frac{10^{20} \text{ eV}}{E_e}\right)$, magnetic fields of $<10^{-11}$ G are sufficiently weak that these synchrotron cooling times become much larger than the 0.3 Mpc ($\sim$1 Myr) interactions lengths (for which the inelasticity per interaction is near unity). Once again, we consider such extreme scenarios in order to capture the effect from a range of parameter space. We refer to this scenario as "*Clark radio, cascade*", presenting the results in the right-hand panel of fig. 4. Furthermore, for this scenario, the development of the e/γ cascades leads to the filling in, and partial erasing, of the dip feature seen previously in the non-cascading result shown in the right-hand panel of fig. 2 in section II.

III. THE PHOTON FRACTION

Since the quantity usually obtained from searches for UHE photons in UHECR data is the photon fraction [24], we present the photon fraction calculated for the "*Clark radio, single*" scenario in fig. 5, obtained by dividing the photon and proton fluxes shown in the two panels of fig. 2. In this plot we also present a breakdown of the contributing photon fluxes to the photon fraction from the different shells. From this breakdown it can be seen that the arriving photon fraction is predominantly contributed from sources in relatively local shells, with distances tens of Mpc away.

The dip feature seen in the photon fraction in fig. 5 originates from a convolution of the GZK feature in the proton flux itself along with the dip feature present in the arriving photon flux explained previously in section 2. For the homogeneous source distribution case, photon fractions between 10^{-3} and 10^{-2} can be seen to be expected, with the photon fraction peaking at 10^{-2} close to the maximum energy the cosmic rays are injected up to before the cutoff kicks in at energy $E_{\max}$. These results are found to be in approximate agreement with previous calculations of the photon fraction [23, 32]. However, this photon fraction result has been calculated for a single maximum energy, $E_{\max}$, of the protons produced by the UHECR sources. In the following section we address the influence other values of $E_{\max}$ have on these results.

A. The Effect of Different Cut-Off Energies

In order to disentangle the effect on the photon fraction caused by the maximum energy of the proton, $E_{\max}$, from the local spatial distribution of UHECR sources to be discussed in this paper, we here explicitly obtain the photon
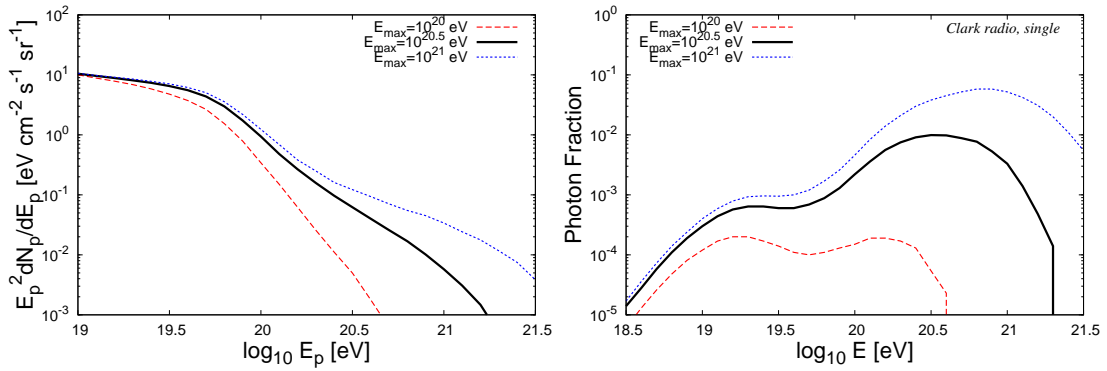
FIG. 6: **Left**: The UHECR proton flux arriving from a homogeneous distribution of sources for different values of $E_{\max}$. **Right**: The corresponding photon fraction of the arriving UHECR obtained from a homogeneous distribution of sources for different values of $E_{\max}$. For this plot, the label "*Clark radio, single*" refers to the assumptions about the radio background and magnetic field strengths, for which we have assumed the Clark et al. [25] radio background and extra-galactic magnetic fields stronger than 0.1 nG. The injected proton spectrum assumed for these results had a spectral index of $\alpha=2$.

fraction for the different $E_{\max}$ values of 10^{20} eV and 10^{21} eV. The alterations to both the GZK feature and the photon fraction are shown in the left and right panels of fig. 6. For comparison we also show the results obtained in the previous sections, with $E_{\max}=10^{20.5}$ eV, in the solid line curves. For all these calculations a homogeneous distribution of sources was assumed. In the left-panel of fig. 6, the effect of the cut-off energy on the arriving UHECR spectrum is shown. An understanding of this effect comes from a consideration of the breakdown of this flux from the different source shells shown in the left-panel of fig. 2, with the cut-off energy primarily effecting the contributions from the more local shells which dominate the UHECR flux at the cut-off energy. In the right-panel of fig. 6, the effect of the cut-off energy on the photon fraction of the UHECR flux is shown. Interestingly, the photon fraction at all energies is seen to increase when the cut-off energy is increased. A qualitative understanding of this follows from the fact that (for a given injection spectrum) as the cut-off energy is increased, the UHECR energy injected into particles above threshold for $p\gamma$ interactions is increased, leading to an increased injection of UHE photons.

However, a more complete understanding as to why the photon fraction increases significantly around the cut-off energy, when the cut-off energy is increased, can be obtained through a consideration of the photon and proton fluxes at the cut-off energy. As the cut-off energy is increased from 10^{20} eV to 10^{21} eV, the proton flux at this energy decreases by nearly an order of magnitude (see the left-panel of fig. 6). Furthermore, the photon flux at the cut-off energy increases by more than an order of magnitude, resulting in more than a two order of magnitude increase in the photon fraction at the cut-off energy. This large increase in the photon flux at the cut-off energy has two components. The first of these may be understood by considering the photon flux produced by protons injected in the 3-9 Mpc and 9-27 Mpc shells, the dominant contributing shells to the arriving photon flux at the cut-off energy. For a cut-off of 10^{20} eV, the majority of the photon flux at the cut-off energy arrives from sources out to $\sim$10 Mpc (ie. only the first Mpc or so of the 9-27 Mpc shell actually contributes), after which attenuation of the flux through pair production interactions kills contributions from sources further away. However, as the cut-off energy is increased to 10^{21} eV, the contributing region to the photon flux at cut-off increases to roughly half the 9-27 Mpc shell (the inner 10 Mpc of the shell), due to the increase of the pair creation interaction length with energy (see the right-panel of fig. 1). Such a contributing region argument leads to a factor of 2 increase in the photon flux. The second, by far the dominant effect causing the large increase in the photon energy flux at the cut-off energy, is the fact that the number flux from a given source at the cut-off energy is the same for the different $E_{\max}$. This follows from the fact that the photon flux at the cut-off energy arrives predominantly from the first pions produced by protons after being emitted from the source (ie. whose distribution follows from $n_{\max}=0$ in eqn (5)). Hence, the energy flux at the cut-off energy, for an order a magnitude in $E_{\max}$, increases by an order of magnitude. The overall effect on the photon fraction is a general increase as the cut-off energy is increased, with the most significant increase occurring for the second peak of the photon fraction curve, which peaks at approximately the cut-off energy, $E_{\max}$.

B. A Local Enhancement/Depression of Cosmic Ray Sources

In the previous section we focussed on the expected results obtained from a homogeneous distribution of sources. In this section we depart from the homogeneous assumption to investigate how the photon fraction is affected by a
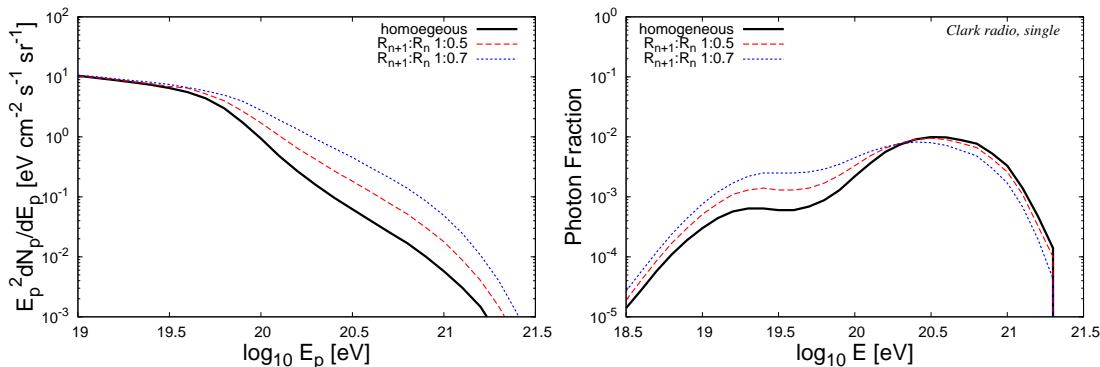
FIG. 7: **Left**: The UHECR energy flux arriving from different distributions of sources for the case of a local source **over-density**. **Right**: The photon fraction of the UHECR flux from different distribution of sources for the case of a local source **over-density**. For this plot, the label "*Clark radio, single*" refers to the assumptions about the radio background and magnetic field strengths, for which we have assumed the Clark et al. [25] radio background and extra-galactic magnetic fields stronger than 0.1 nG. The injected proton spectrum assumed for these results had a cut-off energy of $E_{\mathrm{max}}=10^{20.5}$ eV and an injection spectral index of $\alpha=2$.

local source distribution. In order to account for the natural fluctuations that must exist at some level within the homogeneous distribution locally due to the fact that sources are not distributed continuously in space but are finite in number, occupying particular positions, we here investigate the effect that local source over-densities/under-densities can have on the arriving photon fraction.

In terms of over-densities, for the extreme case in which one of the shell regions dominates completely the arriving UHECR and photon flux above 10^{19} eV, the proton and photon fluxes arriving to Earth would be those from the corresponding shell in fig. 2. From these results, a large photon fraction is found to be achievable for fluxes soley from either local or distant shells, though the energy at which this occurs is very different in the two cases. This will be addressed in section III C. However, typically the expected contribution from each shell should scale approximately with the width of the shell, with contribution ratios of roughly 1.0 : 0.3 : 0.09 : 0.03 : 0.01 being expected. If a local over-density of sources within the surrounding shells considered did exist, the arriving photon fraction and GZK feature would both differ significantly from the homogeneous source distribution scenario. Describing the ratio of the contributing shells as $R_{n+1} : R_n$ (with $n+1$ referring to further away shells), having a ratio of 1:0.3 for the homogeneous source scenario, we alter this ratio in order to simulate the effects of a local over-density, with nearby sources gaining a weighting factor when summing up the shell contributions. In fig. 7, both the effects this has on altering GZK feature (in the left-panel) and the alterations to photon fraction (in the right-panel) are shown. The GZK feature for this scenario is found to be somewhat delayed to higher energies, with a milder cut-off spectral slope, following the increase in dominance of the local contributing shell spectra, whose contributions can be seen in the left-panel of fig. 2. The photon fraction, however, alters only significantly at the lower energy peak, which increases in height with the introduction of the local UHECR source density enhancement, by more than a factor of 2. Such an increase in the photon fraction at lower energies approximately scales with the enhancement ratio of the source distribution locally, as might be expected.

Following on in the vein that a departure from homogeneity might exist in the UHECR source distribution, we also attempt to account for the effect of a local depression in the source distribution by introducing a hole of UHECR sources surrounding Earth. The effects introduced to the GZK feature by a local depression of UHECR sources are shown in the left-panel of fig. 8, with the effects on the photon fraction being shown in the right-panel of fig. 8. Such a depression, in fact, is found to enhance the photon fraction of UHECR, with an increase in the hole size of the sources surrounding Earth, leading to more than an order of magnitude increase in the high energy end ($>10^{20.5}$ eV) of the UHE photon fraction plot. However, it should be noted that such a growth in the photon fraction only exists in the region in which the energy flux of arriving UHE particles is less than 4 orders of magnitude below that at 10^{19} eV, so cannot be expected to be detectable by present UHECR detectors. In this local depression of sources scenario, the GZK feature, contrary to the over-density of sources case, leads to a harder spectral cut-off feature. This is due to the dominance of the further away contributing shells, whose spectra are shown in the left-panel of fig. 2.
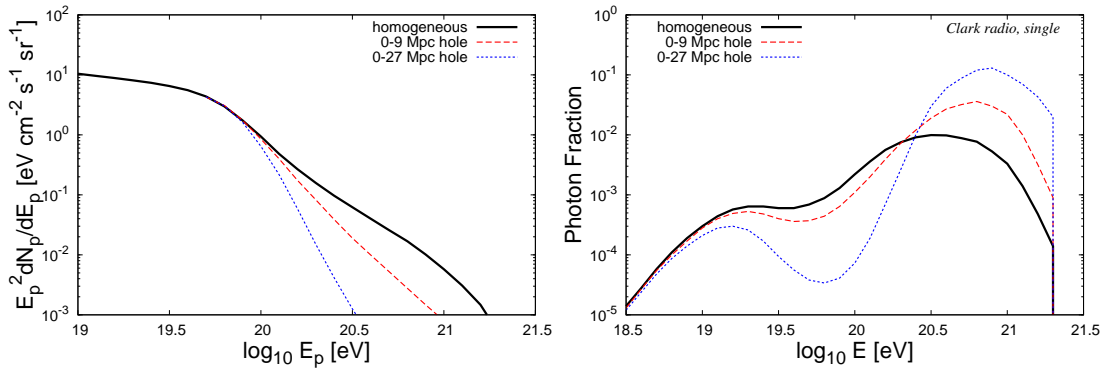
FIG. 8: **Left**: The UHECR energy flux arriving from different distributions of sources for the case of a local source **under-density**. **Right**: The photon fraction of the UHECR flux from different distribution of sources for the case of a local source **under-density**. For this plot, the label "*Clark radio, single*" refers to the assumptions about the radio background and magnetic field strengths, for which we have assumed the Clark et al. [25] radio background and extra-galactic magnetic fields stronger than 0.1 nG. The injected proton spectrum assumed for these results had a cut-off energy of $E_{max}=10^{20.5}$ eV and an injection spectral index of $\alpha=2$.

C. The Photon Fraction from a Single Source

Following on from these perturbations to the source distribution from the homogeneous scenario, we here focus on the photon fraction of the propagating particles from a single UHECR source (assuming rectilinear propagation for protons). This provides an understanding of the photon fraction expected in the extreme scenario of a single dominant local UHECR source. Though this scenario would seem to require uncomfortably slow diffusion in order to prevent violation of anisotropy limits, it nevertheless can provide a useful insight to understand the results obtained from an ensemble of sources located at a particular radius. We show in fig. 9 the evolution of the photon fraction as a function of distance from the UHECR source, for different energy particles. The lines in the plot that terminate early (ie. those for $10^{20.5}$ eV and 10^{21} eV particles) indicate that the energy flux from the source has decreased more than 4 orders of magnitude at the termination distance. Hence, though such a flux may contain a large photon component, it would be unobservable to present generation UHECR detectors. This photon fraction should be considered as a lower bound value, since the presence of magnetic fields will extend the actual propagated path of the protons relative to that of the same energy photons (which themselves have a slight path increase from the source due to their, much higher in energy, parent proton's deflected trajectory).

As a general rule, the photon fraction curves in fig. 9 for particles above the injection cut-off, E_{max}, are different in shape than those below this energy. For particles below E_{max}, the photon fraction curve peaks at more local distances with increasing energy particle. Furthermore, at energies below the peak value, the photon fraction is larger for higher energy particles. This follows simply from a consideration of both the arriving proton and photon fluxes arriving from the different radii shells shown in fig. 2. For particles above E_{max}, the photon fraction in fact curves upwards (has a positive second derivative) with increasing distance. Such an increase in the photon fraction follows from a consideration of our analytic description to both the proton and photon fluxes. Above the energy, E_{max}, at which the injected protons are suppressed, the contribution to the proton fluxes, at a given energy, from the pion losses of higher energy protons, are penalised. Since the photon fluxes of the same energy originate from much higher energy protons, the suppression to the contribution of the photon flux from multi-pion loss protons is also strong. Hence, at energies above the cut-off, the protons that arrive have predominantly undergone no pion production processes and the photon flux arrives predominantly from protons that have only undergone a single pion loss. From this, it follows that the increase in growth of the photon fraction with distance for energies above E_{max} is the result of the decrease in the ability of the protons that have undergone no photo-pion interactions to arrive at Earth and a lack of attenuation of the photons produced by protons that have undergone only a single pion loss. Thus, this rise in the photon fraction, for particles with energy greater than E_{max}, only begins to terminate once the photon flux becomes significantly absorbed through subsequent pair production interactions.
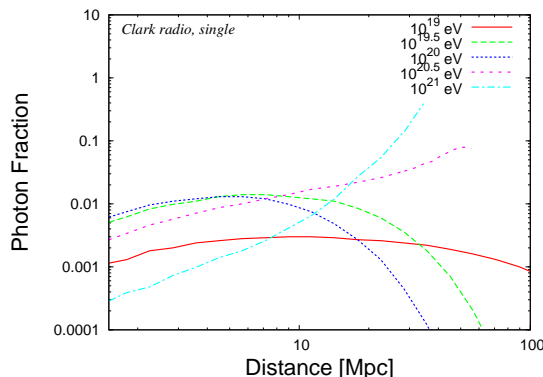
FIG. 9: The photon fraction of UHECR as a function of distance from the source for different arriving energies of photons/protons. For this plot, the label "*Clark radio, single*" refers to the assumptions about the radio background and magnetic field strengths, for which we have assumed the Clark et al. [25] radio background and extra-galactic magnetic fields stronger than 0.1 nG. The injected proton spectrum assumed for these results had a cut-off energy of $E_{\mathrm{max}}=10^{20.5}$ eV and an injection spectral index of $\alpha=2$.

IV.   THE EFFECT OF COSMIC RAY DIFFUSION ON RESULTS

So far in the paper we have ignored the effect introduced by the presence of magnetic fields on the cosmic ray proton trajectories. Without such effects, both UHECR protons and photons propagate rectilinearly from the injection shell to Earth and hence the photon fraction arriving from each shell is as presented in fig. 5 for the homogeneous distribution of sources assumption must be considered a lower bound. However, for consistency with the relatively strong extra-galactic magnetic fields of more than 0.1 nG required for the termination of the e/γ cascade, we here discuss the effects introduced by proton diffusion in the extra-galactic magnetic fields.

As discussed in ref. [3], for Larmor radii significantly larger than the coherence scale of the ordered magnetic field, a charged particle propagating through a uniform magnetic field of coherence length, L_{coh}, will undergo a deflection of size $\alpha=L_{\mathrm{coh}}/R_L$, where R_L is the Larmor radius of the proton. A particle traversing a distance L, through L/L_{coh} randomly oriented magnetic patches of size L_{coh}, will therefore random walk in angle space, being deflected on average by

$$\theta(E_p) \approx \left(\frac{L}{L_{\mathrm{coh}}}\right)^{1/2} \alpha \approx 2.5^{\circ} \left(\frac{10^{19}\ \mathrm{eV}}{E_p}\right) \left(\frac{L}{100\ \mathrm{Mpc}}\right)^{1/2} \left(\frac{L_{\mathrm{coh}}}{1\ \mathrm{Mpc}}\right)^{1/2} \left(\frac{B}{0.1\ \mathrm{nG}}\right). \tag{6}$$

Such angular diffusion leads to the largest increase in path-length the proton propagates, compared to the field-free rectilinear distance, for the "lower energy" protons under consideration. The effect on the proton propagation is to lead to an increased effective distance, L_{eff}, which the protons propagate relative to the straight-line distance, L, with the relative increase given by, $L_{\mathrm{eff}}/L \approx 1 + \theta^2/2$. Thus, a nG strength extra-galactic magnetic field would lead to a $\sim$10% increase in a 10^{19} eV proton's path-length for an L of 100 Mpc.

For the homogeneous distribution of sources scenario, the contribution to the fluxes of protons and photons arriving at 10^{19} eV from different source distances is shown in fig. 2. The arriving proton flux at 10^{19} eV is seen to be dominated by sources beyond several hundred Mpc. Similarly the 10^{19} eV photon flux, which results from roughly 10^{20} eV proton losses, receives its dominant contribution from sources $\sim$100 Mpc at this energy. With the photons propagating rectilinearly to Earth, and the effective proton propagation path being proportional to the inverse square of the proton's energy, the overall path extension of the two routes (p propagation to Earth and $p \rightarrow \gamma$ and subsequent γ propagation to Earth) is dominated by the proton's (ie. first route) path extension. Thus, at 10^{19} eV, the increase in path-length for the protons can be expected to be significantly larger than that of the arriving photons. With the arriving flux from each radial source element being constant for this scenario, the effect of diffusion is to weight the contribution from the more local sources relative to that from the more distant sources. Hence the effect of diffusion, for the homogeneous source scenario, is in fact similar to the case of a local source over-density. For a 0.1 nG field, a resulting mild, $\sim$10%, decrease of the arriving proton flux to the arriving photon flux at 10^{19} eV, leads to a similarly mild increase in the photon fraction $\sim$$10^{19}$ eV relative to the values obtained in the previous sections which ignored magnetic field deflection effects.

Should the UHECR protons be born into a region of large magnetic field, their Larmor radius will be comparable or even smaller than the magnetic field coherence scale (which we here assume to be 1 Mpc). If this occurs, the cosmic

rays propagation may become diffusive, and a consideration of the magnetic field structure on smaller scales should be considered. If such a regime were entered for UHECR close to the source region, the photon fractions expected could be considerably larger than the values obtained here. In this respect, our photon fractions results should be considered as lower bound values.

V.   DISCUSSION

With increasing UHECR proton energy, the sudden onset of the pion-production process $\sim 10^{19.6}$ eV due to a combination of both the low energy resonance-like cross-section for this process and the sharply peaked nature of the CMB's black-body distribution leads to a very sudden decrease in the interaction length for UHECR protons propagating through intergalactic space and consequently a sudden growth of the secondary UHE photon flux produced through these interactions. This, in combination with the relatively large mass of the pion to that of the proton ($m_\pi/m_p \approx 0.15$), results in a sudden decrease also in the attenuation length of UHECR protons. Despite the fact that the UHE photons produced also interact themselves with the CMB photons through a resonance-like cross-section, their interaction length in fact increases with energy due to the Klein-Nishina suppression of these interactions which occur with $s/(m_e c^2)^2 \sim 10^3$ (ie. $\gg 1$), where s is the squared center-of-mass energy of the collision and m_e is the rest-mass of the electron (the propagator in these interactions). As a consequence, the mean-free-path of UHE photons increases with energy, becoming comparable to the attenuation length of protons at 10^{20}-10^{21} eV (depending on the extra-galactic radio background strength assumed), leading to the possibility of a relatively large photon content in the arriving UHECR flux at Earth.

The spectral shape of the GZK feature of the arriving proton flux has been demonstrated to have a very simple to understand origin through an analytic expression for the spatial and energy distributions of protons emitted by a single source, taking into account their subsequent cooling through photo-pion production interactions. Using the individual spectra from the different shells considered, the change in the spectral cut-off feature of the arriving UHECR spectrum was found for both a local over-density and under-density scenario. A local over-density of sources lead to a slight delay to higher energies of this cut-off feature, along with it having softer cut-off spectral shape. On the other hand, for the local under-density scenario, the introduction of a local hole of UHECR sources surrounding the Earth out to ~ 10 Mpc, or even ~ 30 Mpc, lead to a much steeper spectral cut-off feature being obtained.

The photon fraction results obtained, plotted as a function of UHECR energy, was shown to exhibit a double peaked feature. This feature was observed to be present in all scenarios considered (see figs. 5,7,8) provided the extra-galactic magnetic field strength was sufficiently strong (more than ~ 0.1 nG) that the e/γ cascades were prevented from developing, with inverse Compton cooling being out-competed by synchrotron cooling for the UHE electrons. In all cases considered, the higher energy second peak peaked roughly at the cut-off energy of the proton injection spectrum, $E_{\max}$. This being demonstrated to be the case explicitly in fig. 6 for several different values of maximum proton energy, $E_{\max}$. For sufficiently large values of the maximum proton injection energy by the sources ($E_{\max} > 10^{20}$ eV), the higher energy second peak in the photon fraction was larger than the lower energy first peak, with larger values of $E_{\max}$ increasing the height of this peak. Furthermore, the introduction of a hole region around the Earth, void of UHECR sources, lead to a further increase in the photon fraction at this peak value, at energies close to $E_{\max}$. However, the introduction of a local over-density of sources into the nearby (surrounding ~ 250 Mpc) region was found to only mildly reduce this high energy peak in the photon fraction, increasing instead the lower energy peak.

With the prospect of even higher statistic rates at energies above the GZK cut-off with an Auger North detector, information about the UHECR sources through the photon fraction information holds great promise. Already, with the current Auger statistics, the photon fraction limits effectively exclude any, either homogeneous or local, topological origin scenario for UHECR [22, 33]. Following these results, the next step will be the more difficult task of using the photon fraction information to probe the local UHECR source distribution. In this paper, we have investigated possible results expected in this regard, demonstrating that photon fractions in the range 10^{-2}-10^{-3} present realistic lower bound values.

VI.   CONCLUSION

The photon component of the UHECR spectrum has here been demonstrated to be a useful diagnostic tool for:

(1) The origin of a cut-off feature in the observed UHECR spectrum.
Confirmation that the cut-off feature at the high energy end of the UHECR spectrum originates from proton photo-pion interactions with background photons was shown to be promising for a range of radio backgrounds, extra-galactic magnetic field strengths, and cut-off energies, as demonstrated in figs. 4,6.

(2) The local distribution of UHECR sources.

In combination with the GZK cut-off feature, the photon fraction was shown to be a useful tool in the determination of the local UHECR source distribution through the consideration of local source under and over densities, as demonstrated in figs. 7,8.

Acknowledgments

[1] J. Abraham *et al.* [Pierre Auger Collaboration], Nucl. Instrum. Meth. A **523** (2004) 50.
[2] M. Unger and f. t. P. Collaboration, arXiv:0706.1495 [astro-ph].
[3] D. Hooper, S. Sarkar and A. M. Taylor, Astropart. Phys. **27** (2007) 199 [arXiv:astro-ph/0608085].
[4] D. Hooper, S. Sarkar and A. M. Taylor, Phys. Rev. D **77** (2008) 103007 [arXiv:0802.1538 [astro-ph]].
[5] D. Allard, N. G. Busca, G. Decerprit, A. V. Olinto and E. Parizot, arXiv:0805.4779 [astro-ph].
[6] G. R. Blumenthal, Phys. Rev. D **1** (1970) 1596.
[7] K. Greisen, Phys. Rev. Lett. **16**, 748 (1966).
[8] G. T. Zatsepin and V. A. Kuzmin, JETP Lett. **4**, 78 (1966) [Pisma Zh. Eksp. Teor. Fiz. **4**, 114 (1966)].
[9] J. Abraham *et al.* [Pierre Auger Collaboration], Astropart. Phys. **29** (2008) 188 [arXiv:0712.2843 [astro-ph]].
[10] L. Maccione, A. M. Taylor, S. Liberati, D. Mattingly In Prep.
[11] C. D. Dermer, arXiv:0711.2804 [astro-ph].
[12] V. Berezinsky, A. Z. Gazizov and S. I. Grigorieva, Phys. Rev. D **74** (2006) 043005 [arXiv:hep-ph/0204357].
[13] C. C. Lu and G. L. Lin, arXiv:0807.3391 [astro-ph].
[14] D. Hooper, A. Taylor and S. Sarkar, Astropart. Phys. **23** (2005) 11 [arXiv:astro-ph/0407618].
[15] M. Ave, N. Busca, A. V. Olinto, A. A. Watson and T. Yamamoto, Astropart. Phys. **23** (2005) 19 [arXiv:astro-ph/0409316].
[16] R. Engel, D. Seckel and T. Stanev, Phys. Rev. D **64** (2001) 093010 [arXiv:astro-ph/0101216].
[17] R. J. Gould and G. P. Schreder, Phys. Rev. 1404 - 1407 (1967)
[18] G. R. Blumenthal and R. J. Gould, Rev. Mod. Phys. 42, 237 - 270 (1970)
[19] F. A. Aharonian, B. L. Kanevskii, and V. V. Vardanian, Astrophys. Space Sci. **167**, 111A (1990).
[20] R. J. Protheroe and T. Stanev, MNRAS. 264 191 - 200 (1993)
[21] R. J. Protheroe, MNRAS 221 769 - 788 (1986)
[22] F. A. Aharonian, P. Bhattacharjee and D. N. Schramm, Phys. Rev. D **46** (1992) 4188.
[23] G. Gelmini, O. Kalashev and D. V. Semikoz, arXiv:astro-ph/0506128.
[24] J. Abraham *et al.* [Pierre Auger Collaboration], Astropart. Phys. **29** (2008) 243 [arXiv:0712.1147 [astro-ph]].
[25] T. A. Clark, L. W. Brown and J. K. Alexander, Nature 228, 847-849
[26] F. A Aharonian, B. L, Kanevskii, and V. V. Vardanian, Astrophys. Space Sci. **167**, 93A (1990).
[27] S. Karakula, G. Kociolek, I. V. Moskalenko and W. Tkaczyk, Astrophys. J. Suppl. **92** (1994) 481.
[28] F. W. Stecker, Phys. Rev. Lett. 21, 1016 - 1018 (1968)
[29] F. A. Aharonian, A. M. Atoyan, and A, M, Nagapetyan, Astrophysics 19, 187 - 194 (1983)
[30] F. .A. Aharonian and A. M. Atoyan, Astrophys. & Space Science 79 321 - 336 (1981)
[31] R. J. Protheroe and P. L. Biermann, Astropart. Phys. **6** (1996) 45 [Erratum-ibid. **7** (1997) 181] [arXiv:astro-ph/9605119].
[32] O. E. Kalashev, D. V. Semikoz and G. Sigl, arXiv:0704.2463 [astro-ph].
[33] V. Berezinsky, P. Blasi and A. Vilenkin, Phys. Rev. D **58** (1998) 103515 [arXiv:astro-ph/9803271].